coatings

MDPI

Article

Research on the Performance of ZnO Piezoelectric Film Ultrasonic Transducers and Its Application in the Detection of Preload of Hydroelectric Bolts

Xuechao Jing [1], Wenbo Li [1], Ameng Xie [1], Yanghui Jiang [2,*] and Jun Zhang [2,*]

[1] State Grid Hunan Electric Power Company Limited Research Institute, Changsha 410208, China; jxchao2018@gmail.com (X.J.)
[2] School of Power & Mechanical Engineering, Wuhan University, Wuhan 430072, China
* Correspondence: jiangyanghui@whu.edu.cn (Y.J.); zhangjun2010@whu.edu.cn (J.Z.)

Abstract

In this study, ZnO thin-film ultrasonic transducers were directly fabricated by reactive radio-frequency magnetron sputtering for bolt preload detection. The effects of deposition pressure and Ar/O_2 ratio on the morphology, crystal structure, piezoelectric response, and ultrasonic performance of ZnO films were investigated. The ZnO film deposited at 2.0 Pa with an Ar/O_2 ratio of 3:1 exhibited strong c-axis preferred orientation and generated stable high-frequency longitudinal ultrasonic waves with a center frequency above 50 MHz. After being deposited on the bolt surface, the optimized transducer showed a strong linear relationship between ultrasonic time-of-flight and axial load, with an R^2 value greater than 99.99% and an average measurement error below 1% within the preload range. Field monitoring at a hydropower station further showed that the preload variation of randomly selected bolts was negatively correlated with temperature, mainly due to the thermal deformation mismatch between 35CrMo bolts and Q235-B flanges. The maximum preload variation was approximately 40 kN, accounting for about 6.7% of the specified preload of 600 kN, while no abnormal preload loss was observed. These results demonstrate that ZnO thin-film ultrasonic transducers provide a reliable and accurate approach for hydraulic bolt preload measurement and in-service monitoring, with better applicability than conventional torque-based methods.

Keywords: ZnO thin film; deposition pressure; argon-oxygen ratio; ultrasonic longitudinal wave; bolt preload

Academic Editor: Christos Argirusis

Received: 25 June 2026
Revised: 14 July 2026
Accepted: 15 July 2026
Published: 17 July 2026

1. Introduction

Hydroelectric power generation, as an important component of renewable energy, plays a crucial role in ensuring power supply and promoting the green and low-carbon transformation [1,2]. The turbine units are the core electromechanical equipment of hydropower stations, and their safe and reliable operation directly affects the stability and economic efficiency of the power stations. Among the turbine units, the top cover bolts perform a critical function of connecting the turbine top cover with the fixed structure [3]. The magnitude of the preload force of these bolts not only determines the stress state of the bolts themselves but also directly affects the sealing performance and overall structural stability of the top cover [4,5]. Over a long period of operation, the bolts are affected by factors such as vibration, water flow impact, and corrosion. Their axial stress may gradually decrease, leading to bolt loosening or even fracture, thereby causing water leakage, unit shutdown, and even major accidents. Therefore, achieving high-precision online monitoring of the preload force and complex stress states of the bolts is of great significance for ensuring the safe operation of the turbine units.

The methods for measuring the preload of bolts mainly include the torque method, strain gauge method [6], guided wave method, laser grating method [7,8], etc. However, due to issues such as contact friction, threaded plastic-brittle deformation and operational difficulty, these methods have obvious deficiencies in terms of measurement accuracy and practicality. Ultrasonic measurement technology, with its advantages of non-destructiveness, strong penetration, good real-time performance and safety for the human body, is considered an effective means to achieve high-precision measurement of bolt pre-tightening force [9,10]. Its principle is based on the acoustic elasticity effect, that is, changes in the stress state of the material will cause a change in the propagation speed of ultrasonic waves. By measuring the flight time of ultrasonic waves, the axial stress of the bolt can be inversely calculated, thereby evaluating the tightening state of the bolt. The ultrasonic method for measuring bolt stress is divided into two types. One is to directly use the ultrasonic probe to detect the preload of the bolt. This method requires the use of a coupling agent, and the coupling agent will affect the acoustic coupling. The other type involves directly bonding PZT piezoelectric ceramic sheets to the end face of the bolt using epoxy resin or similar adhesive layers [11]. In this method, the thickness of the adhesive layer can affect the detection accuracy. What is more important is that the piezoelectric ceramic sheets are highly brittle, and they are prone to cracking during installation and use. Directly depositing piezoelectric film transducers on the polished end face of the bolt and integrating them into an intelligent bolt is an effective solution to the aforementioned problems [12,13].

In recent years, zinc oxide (ZnO) piezoelectric films have attracted much attention as ultrasonic transducer materials in the measurement of bolt preload force [14]. ZnO has a hexagonal wurtzite structure, and its piezoelectric properties depend on crystal orientation rather than polarization treatment [15]. At the same time, its preparation temperature is low, the thickness uniformity is good, and the mechanical stability is high, making it suitable for directly fabricating film sensors on the bolt surface [16]. Through radio frequency magnetron sputtering, a stable ZnO film can be formed on the bolt surface, achieving metallurgical bonding with the bolt, thus eliminating the need for coupling agents or drilling, and solving the problems of poor adhesion, cumbersome operation and large signal loss existing in traditional patch or probe methods. During the film preparation process, the deposition process parameters significantly affect the crystal orientation and ultrasonic response performance of the film, thereby affecting the excitation effect of longitudinal and transverse waves and the measurement accuracy [17,18].

Although ZnO thin-film ultrasonic transducers have been reported for bolt stress and preload measurement, most previous studies have remained at the laboratory verification stage, mainly involving film preparation, ultrasonic response testing, and load calibration under controlled conditions. However, the long-term field monitoring performance, service stability, and measurement accuracy of ZnO thin-film sensors in actual engineering environments have rarely been investigated. This limitation is particularly important for hydropower turbine bolts, where temperature variation, vibration, structural constraints, and long-term service conditions may affect ultrasonic signal stability and preload estimation reliability. For the complex stress state and long-term service environment of the top cover bolts of the hydroelectric generator set, developing high-performance, high-reliability and high-precision ZnO film ultrasonic sensors is of great significance for realizing the full life cycle health monitoring of bolt. This research will be based on the ZnO piezoelectric film material, systematically exploring the influence of the film preparation process on ultrasonic performance, providing technical support and theoretical basis for online stress detection and safety warning of bolts in hydroelectric generator sets. Therefore, the key advance of this work lies not only in optimizing the ZnO thin-film transducer and calibrating its preload measurement performance but also in verifying its applicability through field monitoring at a hydropower station. By analyzing the preload variation of randomly selected bolts and the corresponding temperature response during service, this study provides a more practical evaluation of ZnO thin-film ultrasonic transducers for long-term bolt preload monitoring.

2. Experiment Details

ZnO piezoelectric thin films were deposited by RF magnetron sputtering onto three types of substrates: (100)-oriented single-crystal Si wafers with a thickness of 0.5 mm, 304 stainless-steel substrates with a thickness of 0.8 mm, and M56 × 330 mm hydraulic bolts. The detailed deposition conditions are listed in Table 1. A high-purity ZnO ceramic target, measuring 150 mm in diameter and 8 mm in thickness, with a purity of 99.99%, was used as the sputtering source. Before the experiment, the substrate was ultrasonically cleaned in alcohol for 10 min, dried, and placed on the sample holder. The distance between the substrate and the target was controlled at 60 mm. The vacuum chamber was heated to 150 °C, the pressure was reduced to 7×10^{-3} Pa, argon gas was introduced (purity 99.99%), the bias voltage and arc power were turned on, and plasma etching was performed on the substrate under the conditions of −150 V, duty cycle 50%, pressure 1.0 Pa, and current 90 A to remove the impurities attached to the substrate surface. After the etching, argon and oxygen (purity 99.99%) mixed gas was introduced, and the radio frequency power was controlled at 600 W to prepare the ZnO piezoelectric film. A sequential single-factor experimental design was adopted. First, the deposition pressure was varied from 1.0 to 2.5 Pa, while the Ar/O_2 flow ratio was kept constant at 1:1 to determine the appropriate sputtering pressure. Subsequently, under the optimized sputtering pressure, the Ar/O_2 ratio was varied from 1:3 to 3:1 to further optimize the ZnO thin-film transducer.

Table 1. Preparation parameters of different thin films.

Experimental Parameters	ZnO	SiO_2	Cr	AgCr
Temperature/°C	150	150	80	80
Target substrate distance/mm	60	70	140	70
Sputtering pressure/Pa	1.0, 1.5, 2.0, 2.5	1.5	1.0	1.0
Argon-oxygen ratio	1:3, 1:2, 1:1, 2:1, 3:1	1:1	1:0	1:0
Sputtering time/h	4	4	0.03	1
Sputtering power/W	600	650	/	700

A piezoelectric ultrasonic sensor was obtained by preparing electrodes on the ZnO film surface. For the ultrasonic response tests on stainless-steel substrates, the ZnO film was directly deposited on the 304 stainless-steel substrates, and a silver paste electrode was applied on the surface of the ZnO film as the top electrode; the structural diagram is shown in Figure 1a. For the bolt sensor, a more stable multilayer electrode structure was fabricated to meet the requirements of field application. Figure 1b illustrates the electrode configuration fabricated on the bolt end face. The multilayer structure of the bolt transducer and the pulse-echo ultrasonic measurement system are shown in Figure 1c. After the ZnO piezoelectric film was deposited on the bolt end face, a dense SiO_2 insulating and protective layer was prepared by magnetron sputtering. Subsequently, a Cr bonding layer was deposited on the SiO_2 layer by arc ion plating to improve the adhesion of the upper electrode. Finally, an AgCr electrode was deposited by magnetron sputtering using

https://doi.org/10.3390/coatings16070855

an AgCr target with an atomic ratio of 7:3. The specific deposition parameters are shown in Table 1.

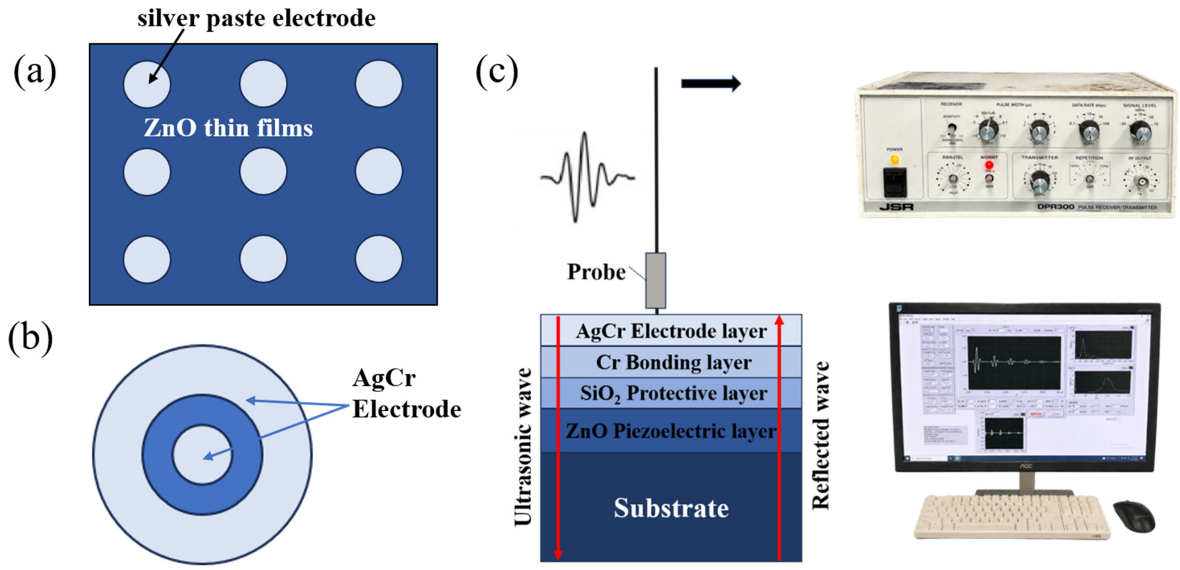

Figure 1. ZnO thin-film ultrasonic transducer and ultrasonic measurement system: (**a**) silver-paste electrodes fabricated on the ZnO thin film deposited on a 304 stainless-steel substrate; (**b**) electrode configuration fabricated on the bolt end face; and (**c**) cross-sectional structure of the bolt transducer and the pulse-echo ultrasonic measurement system.

The Si wafer was mainly used for the characterization of film morphology, thickness, chemical composition, and crystal structure because of its flat surface and low roughness, which are favorable for SEM and XRD analysis. The 304 stainless-steel substrate was used to evaluate the ultrasonic response of the ZnO thin-film transducer, since it is conductive and can serve as the bottom electrode, and its metallic acoustic characteristics are closer to those of the bolt. This paper used a SmartLab SE X-ray diffractometer (Rigaku Corporation, Akishima, Japan) to characterize the structure of the prepared ZnO piezoelectric film materials. The X-ray source was Cu Kα, and the sampling range was 20–80°. A field emission scanning electron microscope of the MIRA3 model (TESCAN GROUP, a.s., Bohunice, Czech Republic), was used to characterize the surface and cross-section of the sample, and the thickness of the coating was measured. The composition elements of the sample were determined using an energy dispersive spectrometer (EDS) (Oxford Instruments, High Wycombe). The room-temperature piezoelectric coefficient d_{33} was determined using an SA1303A piezoelectric tester (Wuxi ShiAo Technology Co., Ltd., Wuxi, China). Ultrasonic responses produced by the ZnO thin-film transducer were acquired with a self-developed pulse-echo receiving system, as illustrated in Figure 1. During testing, the transducer was excited by a 100 V spike pulse with a duration of 70 ns. The generated ultrasonic wave propagated through the substrate was reflected from the opposite surface, and then returned to the same transducer, where it was converted into an electrical echo signal. The received signal was conditioned using a 12.5 MHz low-pass filter and a 60 MHz high-pass filter together with signal amplification. Bolt axial-load calibration was performed on a WAW-300 universal testing machine (Shanghai Precision Instrument and Metering Co., Ltd., Shanghai, China) by gradually applying tensile load until the predetermined force level was reached. At the same time, the acoustic time and bolt temperature during the ultrasonic wave propagation inside the bolt were recorded. The axial force calibration range of the bolt was 0 kN to 600 kN, and data were collected and recorded at intervals of 60 kN.

3. Results and Discussion

3.1. Effect of Deposition Pressure on the ZnO Films

Figure 2 shows the surface and cross-sectional morphologies of ZnO films deposited at different working pressures while the Ar/O_2 flow ratio was fixed at 1:1. For each deposition pressure, there are two high-magnification and low-magnification surface morphology and cross-sectional morphology images. At a deposition pressure of 1.0 Pa (Figure 2a), the film surface presents relatively rough and irregular particles, accompanied by obvious agglomeration phenomena, resulting in uneven surface texture. This morphology indicates that under the condition of high atomic kinetic energy, rapid nucleation and competitive grain growth phenomena are significant. When the deposition pressure increases to 1.5 Pa (Figure 2b), the surface becomes significantly more uniform, presenting closely arranged fine particles with a narrow particle size distribution. This refinement of the grain structure indicates an increase in nucleation density and more uniform lateral grain growth. Further increasing the deposition pressure to 2.0 Pa (Figure 2c), the ZnO film presents a smooth and dense surface composed of closely arranged regular particles, with nearly spherical grains, which is the typical surface morphology of the film showing (002) growth. This indicates that its growth state is stable. At a deposition pressure of 2.5 Pa (Figure 2d), the film surface shows spherical grain growth with large and small particles growing in a mixed manner. This is due to the excessive collision frequency in the plasma reducing the average free path of particles, thereby reducing the migration energy of particles and causing uneven microscopic morphology along the growth direction [19]. The cross-sectional SEM images in Figure 2 show that all ZnO films present a typical columnar crystal structure, which runs throughout the entire film thickness and is a typical feature of sputtering-prepared ZnO films. For films deposited at lower pressures, the columnar crystal structure appears to be relatively loose, with obvious inter-column gaps, and the columnar grains are relatively coarse, which is attributed to the influence of high-energy particle bombardment and re-sputtering effects. As the deposition pressure increases to 2.0–2.5 Pa, the columnar structure becomes more vertically aligned and densely arranged, indicating that the shadow suppression effect has been enhanced and the continuity of the columnar structure has also been improved [20].

Figure 3a shows the thickness of the ZnO film measured from the cross-sectional SEM images and the calculated deposition rate under different deposition gas pressures. The thickness of the film varies with the change in deposition gas pressure, but the variation is not very significant. At lower deposition gas pressures, the kinetic energy of the sputtering particles is larger, the average free path is higher, and the substrate's ability to constrain the arriving particles is poorer. The re-sputtering effect causes the deposition thickness of the film to decrease. When the deposition gas pressure continues to increase to 1.5 Pa, this is the maximum thickness of the film. When the deposition gas pressure continues to increase to 2.0 Pa, the thickness of the film decreases. This phenomenon can be attributed to the competition between the enhanced sputtering yield at higher pressures and the increased gas-phase scattering, where excessive gas molecule collisions reduce the kinetic energy of the sputtering particles and limit the effective growth of the film. When the gas pressure continues to increase to 2.5 Pa, the flux of particles reaching the substrate increases, and the thickness shows an upward trend. Figure 3b shows the elemental composition of the ZnO film surface measured by EDS at a magnification of 20k. The surface of the film only detects the components of Zn and O. Considering the limited accuracy of EDS in quantifying light elements such as oxygen, the measured Zn and O contents should not be regarded as the exact stoichiometric ratio of the ZnO films. The results indicate that the overall elemental composition remained relatively stable with changing deposition pressure, although slight variations in the apparent Zn/O ratio were observed.

https://doi.org/10.3390/coatings16070855

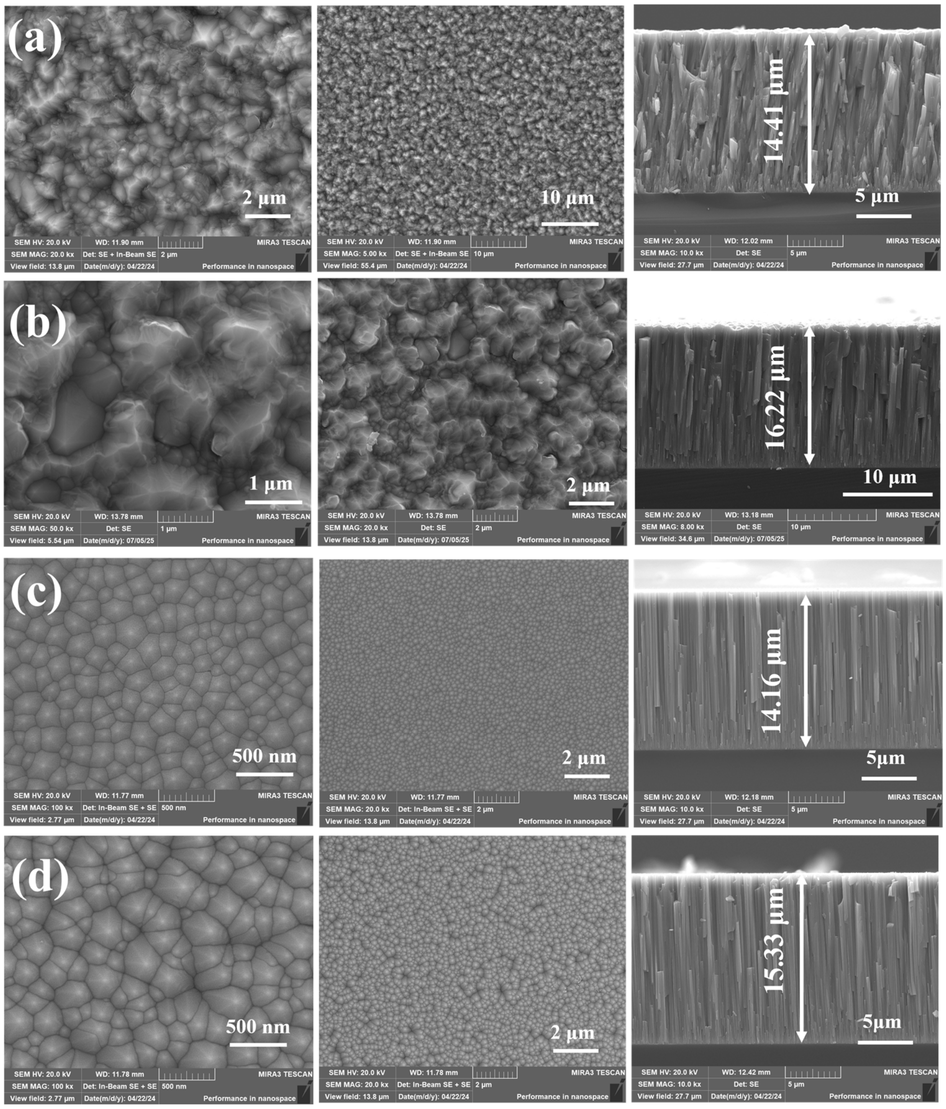

Figure 2. The morphology of ZnO thin films deposited on Si wafers under different deposition pressures. (**a**) 1.0 Pa; (**b**) 1.5 Pa; (**c**) 2.0 Pa; (**d**) 2.5 Pa.

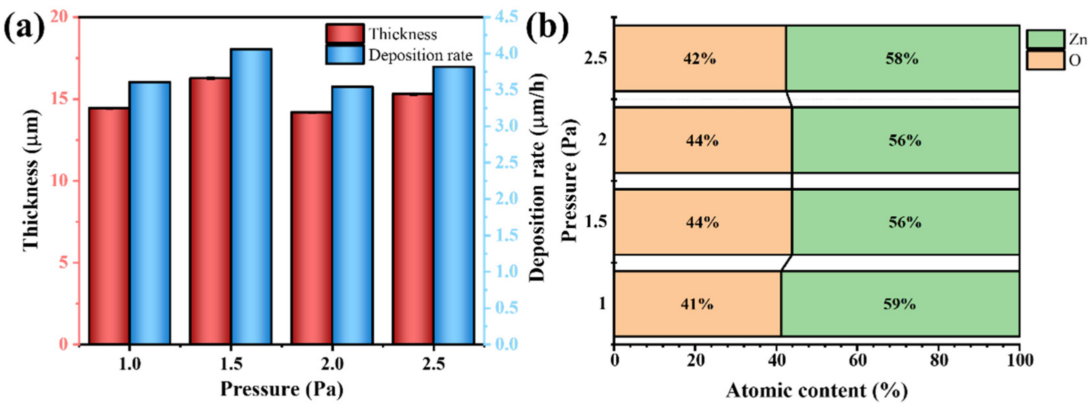

Figure 3. (**a**) Thickness and deposition rate of ZnO films under different deposition pressures; (**b**) surface elemental composition.

The pressure of the sputtering gas has a crucial influence on the growth behavior of ZnO films. Figure 4a shows the XRD patterns of ZnO films prepared under different deposition gas pressures. From the Figure 4a, it can be seen that when the deposition gas pressure is 1.0 Pa and 1.5 Pa, the XRD results of the films show diffraction peaks of

(100), (002), and (101). When the gas pressure is lower, the sputtered atoms have a larger average free path and stronger impact ability on the substrate, and the deposition rate of the film increases, which is conducive to the formation of the (100) orientation [21]. When the deposition gas pressure is 2.0 Pa and 2.5 Pa, the XRD patterns show a single (002) diffraction peak. This indicates that the increase in deposition gas pressure is beneficial to the coating, showing c-axis oriented growth. Based on the atomic arrangement theory of crystal planes, there are significant differences in the surface density of oxygen atoms on different oriented crystal planes of ZnO films [22]. Among them, the oxygen atom surface density of the (100) crystal plane is the lowest, while the (002) and (110) crystal planes show a higher oxygen atom enrichment degree. Under low deposition gas pressure conditions (1.0–1.5 Pa), the sputtering particles have a longer average free path, thus maintaining a higher kinetic energy, making Zn atoms more inclined to nucleate and grow on the oxygen atom relatively sparse (100) crystal plane. During this process, the continuous bombardment of high-energy particles on the substrate surface weakens the thermodynamic stability of the film growth system, making the crystal orientation mainly regulated by dynamic factors and promoting the formation of a metastable structure limited by dynamic conditions [23]. When the deposition gas pressure increases by 2.0 Pa, the collision frequency of particles in the plasma increases, and the energy loss increases accordingly, resulting in a significant decrease in the kinetic energy of the particles, and the film growth process gradually shifts from being dominated by dynamics to being dominated by thermodynamics. Under this condition, the oxygen atom dense crystal plane gains growth advantage driven by the minimization of surface energy.

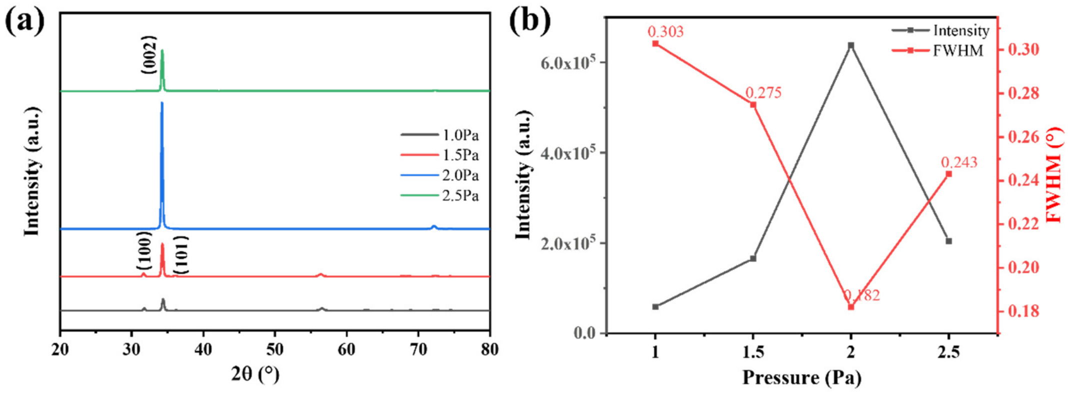

Figure 4. Structure of ZnO thin films with different deposition pressures. (**a**) XRD patterns; (**b**) intensity and FWHM of (002) diffraction peak.

To further explore the influence of deposition gas pressure on the c-axis orientation of the film, the results of the intensity and full width at half maximum (FWHM) of the (002) diffraction peak are presented in Figure 4b. From the Figure 4b, it can be seen that the intensity of the (002) diffraction peak of the film first increases and then decreases, and the FWHM first decreases and then increases, reaching the maximum diffraction peak intensity and the minimum FWHM at 2.0 Pa. At lower pressures, the sputtered particles retain excessively high kinetic energy, and strong bombardment and re-sputtering disturb the ordered growth of ZnO grains, resulting in multiple crystallographic orientations. At 2.0 Pa, gas-phase collisions moderately reduce the particle energy, suppressing excessive bombardment while maintaining sufficient surface mobility for atomic rearrangement. Consequently, a larger proportion of ZnO crystallites grow preferentially along the c-axis, leading to improved orientation consistency and a substantial increase in the (002) peak intensity. When the pressure is further increased to 2.5 Pa, excessive scattering reduces the energy and surface diffusion ability of the arriving particles, thereby weakening the ordered growth of the (002)-oriented grains and decreasing the diffraction peak intensity. The FWHM of the ZnO (002) peak is related not only to crystallite size but also to microstrain, residual stress, defect density, lattice distortion, and orientation distribution. The lowest FWHM at 2.0 Pa indicates improved crystallinity, lower lattice distortion and defect density, and a more ordered c-axis preferred orientation. At lower pressures, excessive particle bombardment and re-sputtering may introduce defects and stress fluctuation, while at higher pressures, gas-phase scattering reduces the energy of arriving particles and weakens surface diffusion, both of which can contribute to peak broadening.

Figure 5 shows the ultrasonic response performance and the piezoelectric constant d_{33} of ZnO films under different deposition gas pressures. The ultrasonic signals excited by the ZnO films prepared under different deposition gas pressures are shown in Figure 5a. From the Figure 5a, it can be seen that the deposition gas pressure has a significant effect on the signal excitation of the ultrasonic films. All films can excite obvious ultrasonic echo signals, which confirms the effective electromechanical coupling of the ZnO film transducer. The ultrasonic waves excited by the ZnO films prepared under 1.0 Pa and 1.5 Pa deposition gas pressures have obvious differences from those excited by the ZnO films prepared under 2.0 Pa and 2.5 Pa deposition gas pressures. According to the ultrasonic wave speed being equal to the substrate thickness divided by twice the flight time, two types of ultrasonic waves can be calculated: one is the faster longitudinal wave (LW), and the other is the slower transverse wave (SW). The ultrasonic waves excited by the films under 1.0 Pa and 1.5 Pa deposition gas pressures are mainly longitudinal waves, and there is also the excitation of a lower amplitude longitudinal wave, which is related to the (100) and (101) multi-directional growth of the film. The growth of the (100) crystal plane of the film is parallel to the substrate direction, and this structure can excite ultrasonic transverse waves perpendicular to the pointing direction. Due to the multi-directional growth structure of the film, ultrasonic longitudinal and transverse waves can be excited under 1.0–1.5 Pa deposition gas pressures. At 2.0–2.5 Pa deposition gas pressures, the ultrasonic waves excited by the film are longitudinal waves [24]. Figure 5b shows the frequency diagram of the ZnO film under 2.0 Pa deposition gas pressure. The echo amplitude can be clearly seen from the Figure 5b. The waveform is a narrow pulse-echo signal, with a central frequency of approximately 57 MHz, which is characteristic of a high-frequency ultrasonic transducer. The highest signal amplitude and the central frequency under the ultrasonic echo are plotted for different deposition gas pressures of ZnO films, as shown in Figure 5c. The ZnO films exhibit a small relative amplitude at lower gas pressures, with the film's signal amplitude being the highest at 2.0 Pa. All samples under different deposition gas pressures exhibit a central frequency of 50 MHz or above, which is characteristic of a high-frequency ultrasonic. Figure 5d shows the piezoelectric constant d_{33} of ZnO films under different deposition gas pressures. At lower gas pressures of 1.0–1.5 Pa, the d_{33} piezoelectric constant of the film is very small, basically less than 3 pC/N, which is related to the (100) crystal plane growth of the film. With the increase in the gas pressure to 2.0 Pa, the d_{33} value of the film reaches the maximum, which is related to the strong c-axis orientation of the film. The variation law of the observed ultrasonic performance with the working pressure can be attributed to the combined effect of crystal orientation, the integrity of the microstructure, and the piezoelectric coupling efficiency. At 2.0 Pa deposition gas pressure, sufficient kinetic energy and surface diffusion of atomic clusters promote the growth of highly oriented (002) orientation, which is crucial for maximizing the longitudinal piezoelectric response of ZnO. In addition, the ultrasonic signal amplitude is directly related to the film's piezoelectric performance, which can be proven from the corresponding d_{33} values.

https://doi.org/10.3390/coatings16070855

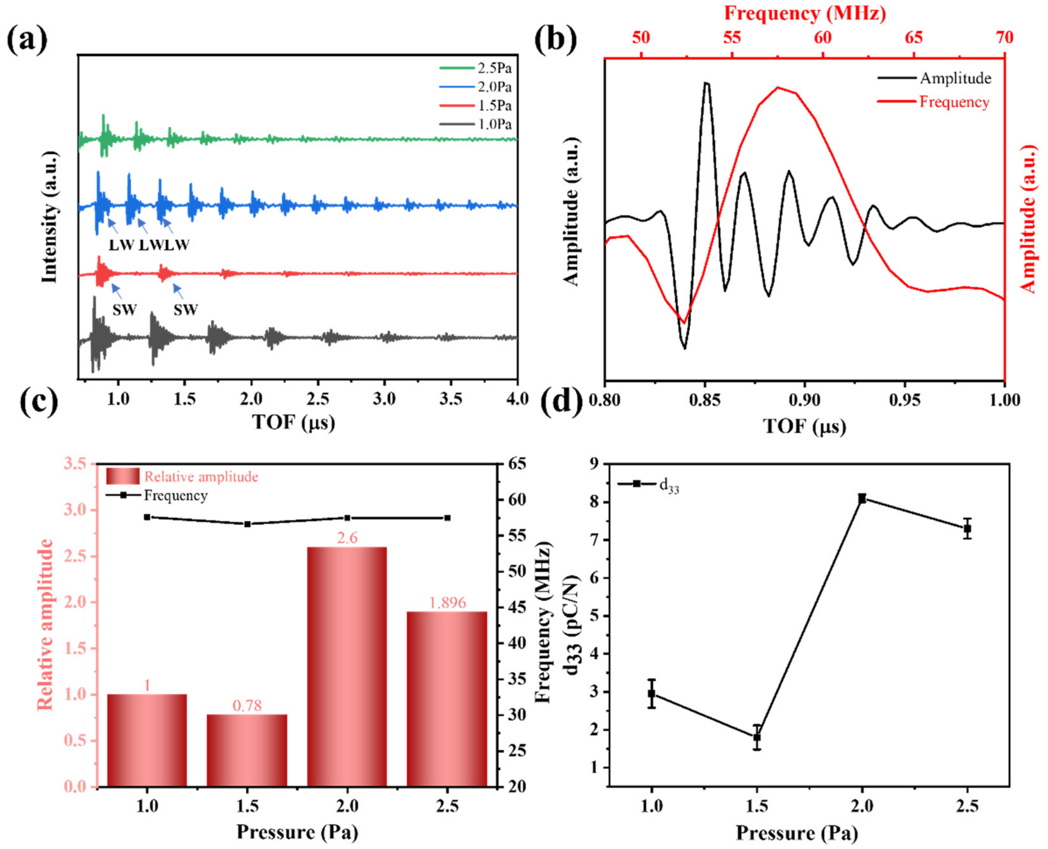

Figure 5. (**a**) Ultrasonic pulse-echo response of ZnO film deposited on SS wafers at different deposition pressures; (**b**) spectral diagram at 2.0 Pa; (**c**) relative amplitude and Frequency; (**d**) d_{33}.

3.2. Effect of the Ar/O_2 Ratio on the ZnO Films

In order to study the influence of the argon-oxygen ratio on the ZnO film, we chose to continue the research under the optimal deposition pressure of 2.0 Pa as described in Section 3.1. Figure 6a–e show the SEM surface morphology of the ZnO films prepared under different argon-oxygen ratios. Under the argon-oxygen ratio condition (Figure 6a), the film surface is composed of small-sized, uniformly distributed spherical grains with clear grain boundaries. When the flow ratio is adjusted to 1:2 and 1:1 (Figure 6b,c), the surface grain size significantly increases, the grain contour becomes more regular, the grain boundaries are clear, and the film surface has good density. This indicates that with the increase in the argon proportion, the kinetic energy of the sputtered particles increases, the surface diffusion ability improves, and it is conducive to the merging and preferential growth of grains [25]. Further increasing the argon proportion to 2:1 and 3:1 (Figure 6d,e), the surface grains continue to coarsen, and at the 3:1 condition, the grain size of the film is the largest, and the surface grains of the film present a uniform and regular arrangement. From the cross-sectional morphology of the film, all samples show obvious columnar crystal growth characteristics, with the columnar crystals arranged perpendicularly to the substrate direction, which is consistent with the particle state extending to the surface.

Figure 7a shows the changes in the thickness and deposition rate of the ZnO films prepared under different argon-oxygen ratios. As the argon/oxygen flow ratio increases, the thickness and deposition rate of the films show a trend of first increasing and then decreasing. With the increase in the argon partial pressure, the particle energy increases, and the thickness and deposition rate of the films increase. When the argon/oxygen flow ratio further increases to 3:1, there is a slight downward trend in the thickness and deposition rate of the films, which may be due to the enhanced re-sputtering effect causing a decrease in the film thickness. The EDS analysis results of the ZnO films on the surface under different argon-oxygen ratios are shown in Figure 7b. The content of Zn and O elements on the surface of the ZnO films is close to the stoichiometric ratio, and the variation amplitude with the argon/oxygen flow ratio is small, indicating that the overall chemical composition of the films remains stable during the deposition process.

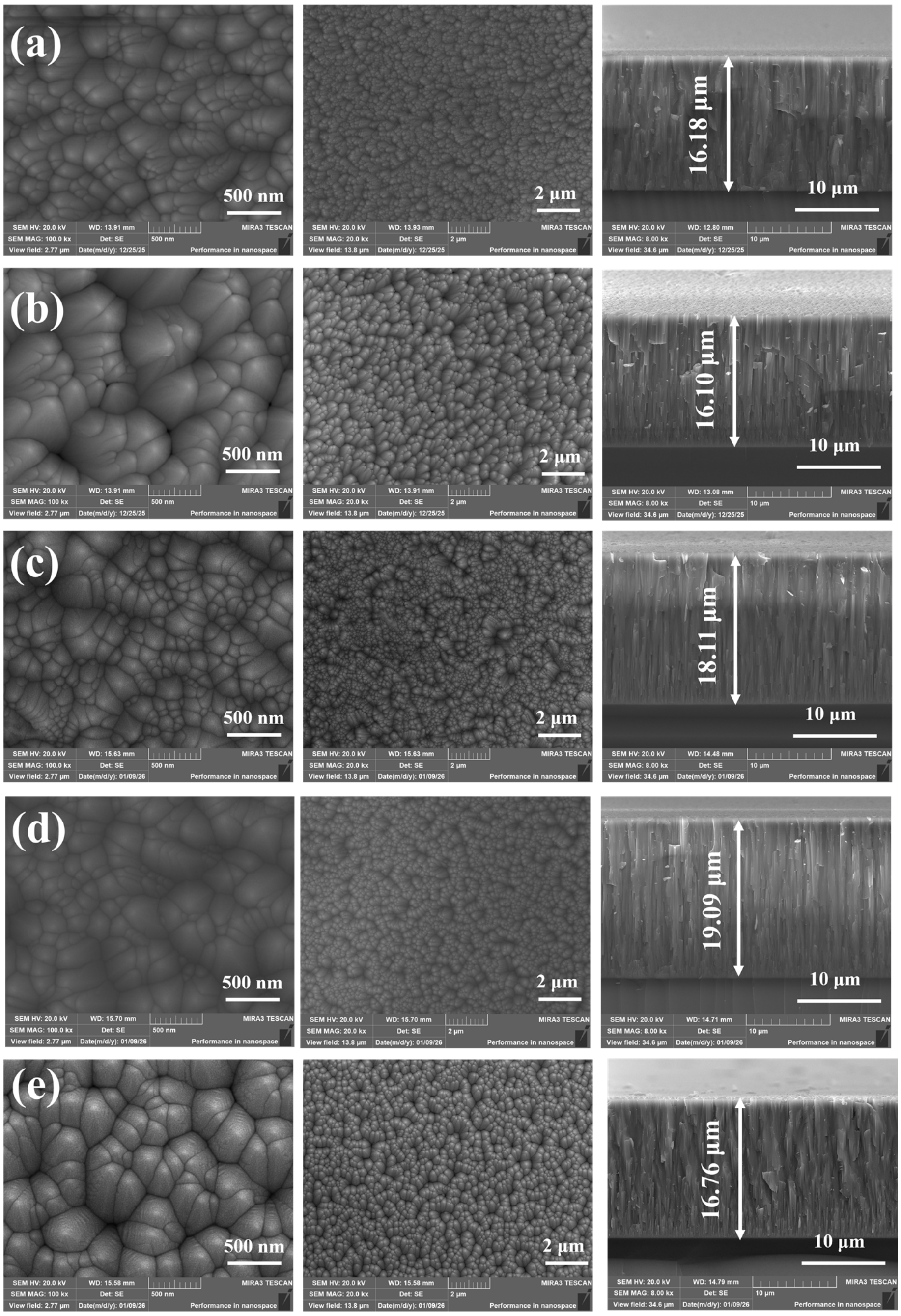

Figure 6. The morphology of ZnO thin films deposited on Si wafers under different argon-oxygen ratios. (**a**) 1:3; (**b**) 1:2; (**c**) 1:1; (**d**) 2:1 and (**e**) 3:1.

Figure 8a shows the XRD patterns of ZnO films deposited under different argon-oxygen ratios. From the Figure 8a, it can be seen that the ZnO films all exhibit a clear ZnO (002) diffraction peak at $2\theta \approx 34.4^{\circ}$, indicating that the prepared films all present a typical hexagonal wurtzite structure and grow preferentially along the c-axis [26]. The intensity and FWHM of the (002) diffraction peak of the films are shown in Figure 8b. With the increase in argon partial pressure, the intensity of the (002) diffraction peak of the films gradually increases, and the FWHM gradually decreases, indicating an improvement in crystallization quality. At lower argon-oxygen ratios, the (002) peak intensity is weak and the half-width is large, indicating poor film crystallization quality, small grain size, and high internal defect density. This is attributed to the fact that excessive oxygen in the film will be trapped at the grain boundaries, hindering the growth of grains, and excessive oxygen will increase the internal defects in the film, thereby reducing the crystallization quality of the film [27]. When the argon-oxygen ratio is higher than 1:1, the addition of O_2 can compensate for the oxygen vacancies in the film, reduce lattice distortion, and promote the preferential growth of ZnO crystals along the energy-minimum (002) crystal plane, improving the crystallization quality of the film [28]. The film shows the optimal (002) preferential orientation growth at an argon-oxygen ratio of 3:1.

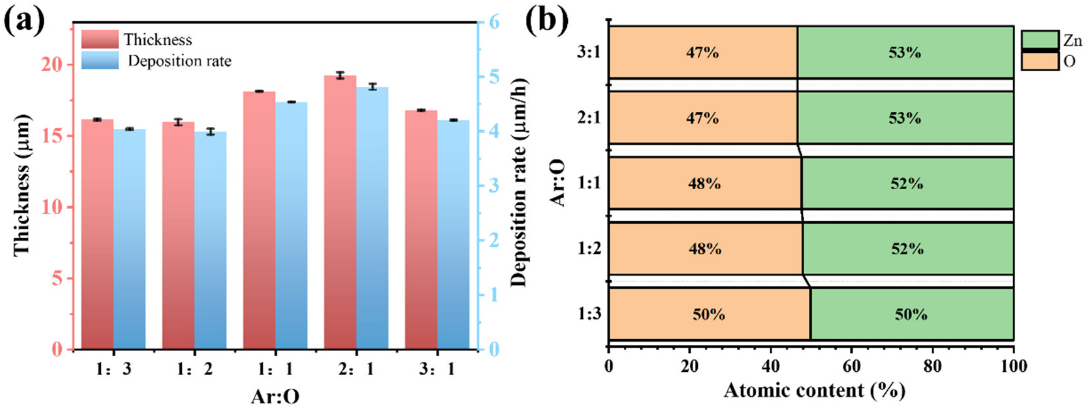

Figure 7. (**a**) Thickness and deposition rate of ZnO films under different argon-oxygen ratios; (**b**) surface elemental composition.

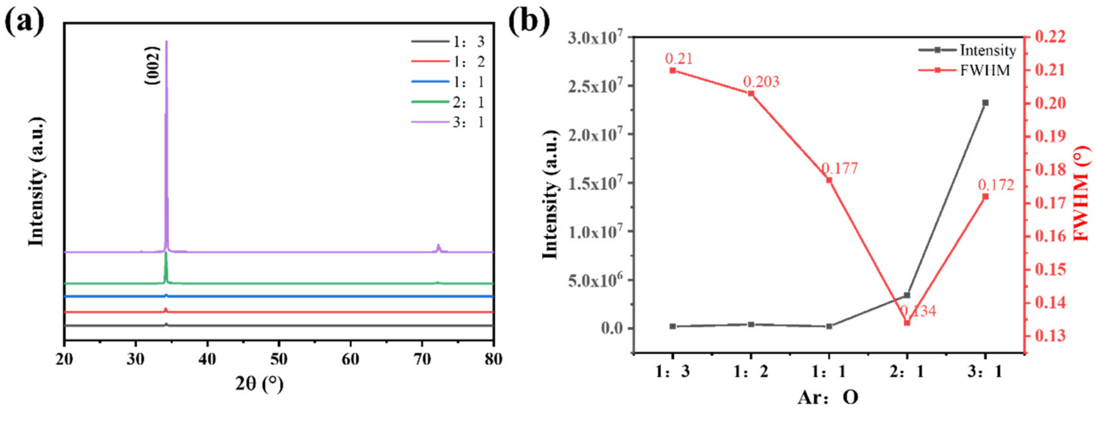

Figure 8. Structure of ZnO thin films with different argon-oxygen ratios. (**a**) XRD patterns; (**b**) intensity and FWHM of (002) diffraction peak.

Figure 9a shows the excited ultrasonic time-domain echo signals of ZnO films prepared under different argon-oxygen ratios. As the argon-oxygen ratio changes, the films can all excite ultrasonic longitudinal waves, which is related to the pure c-axis preferred orientation of the films. Figure 9b is the frequency diagram of ZnO films under an argon-oxygen ratio of 3:1. From the Figure 9b, the echo amplitude can be clearly observed. This waveform shows a narrow pulse-echo signal, with a central frequency of approximately 54 MHz, still showing the characteristics of a high-frequency ultrasonic transducer. The highest signal amplitude and the central frequency of the ultrasonic echo under different argon-oxygen ratios for ZnO films are plotted as shown in Figure 9c. As the argon partial pressure increases, the amplitude of the excited ultrasonic signal of the films gradually increases, and it reaches the maximum relative amplitude at an argon-oxygen ratio of 3:1. This is related to the c-axis orientation of the films, which can be verified from the XRD results. All samples prepared under different Ar/O_2 ratios exhibited center frequencies above 50 MHz, which are comparable to those reported for high-frequency ZnO thin-film ultrasonic transducers and confirm their effective high-frequency ultrasonic response. Figure 9d shows the piezoelectric constant d_{33} of the ZnO films deposited under different Ar/O_2 ratios. As the Ar partial pressure increased, the d_{33} value gradually increased and reached a maximum of 8.3 pC/N. This value falls within the reported range of 5.9–12.4 pC/N for sputtered ZnO thin films, indicating that the optimized film possesses favorable piezoelectric properties [29]. As the argon-oxygen ratio gradually increases, the amplitude of the ultrasonic echo signal significantly increases, and the main resonance peak in the spectrum becomes clearer and the amplitude significantly increases. At the same time, the d_{33} piezoelectric constant value shows a continuous upward trend, indicating that the piezoelectric performance of the films has been effectively improved. This phenomenon is consistent with the trend of enhanced (002) preferred orientation and reduced FWHM in the XRD results mentioned above, indicating that the improvement of c-axis orientation and the improvement of grain quality are the main reasons for the enhancement of piezoelectric performance [30].

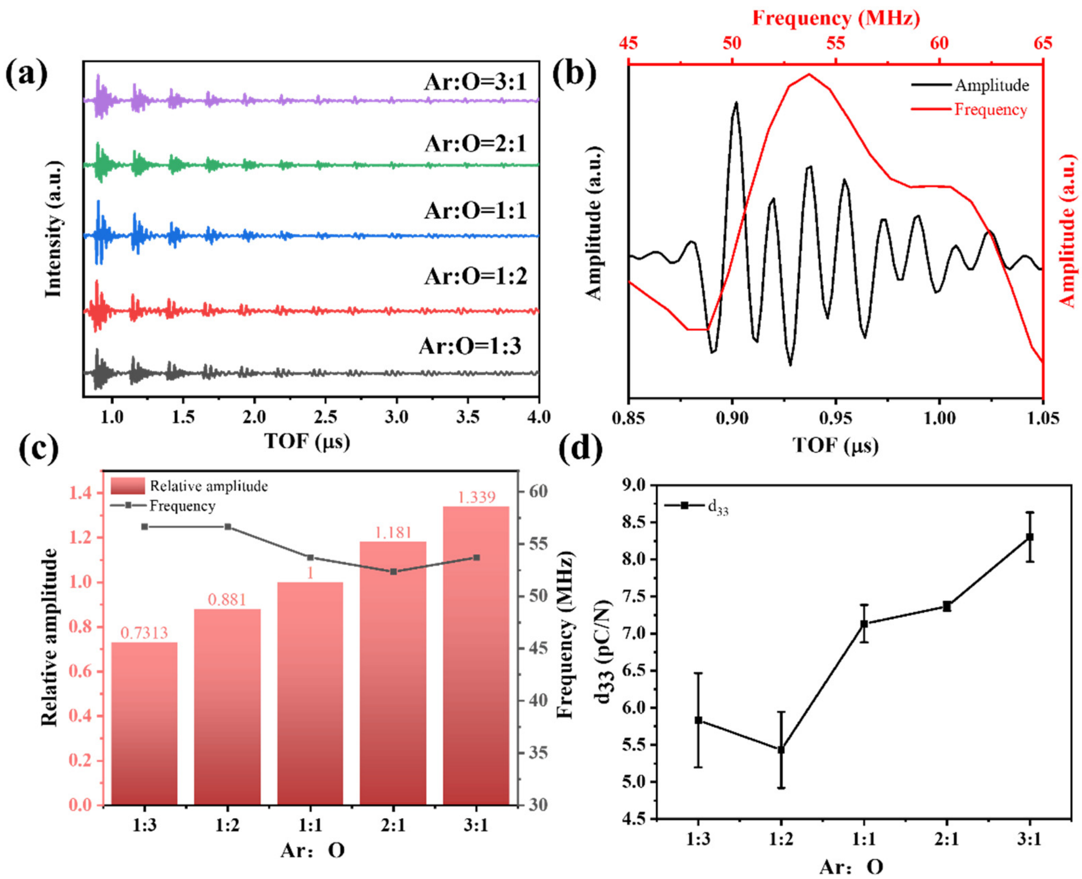

Figure 9. (**a**) Ultrasonic pulse-echo response of ZnO film deposited on SS wafers at different argon-oxygen ratios; (**b**) spectral diagram at argon-oxygen ratio is 3:1; (**c**) relative amplitude and frequency; (**d**) d_{33}.

3.3. Application of the ZnO Thin-Film Transducer for Bolt Preload Monitoring

In order to verify the real-time application capability of the ZnO film transducer, the optimal deposition parameters were selected: a deposition pressure of 2.0 Pa and an argon-oxygen ratio of 3:1. The ZnO film transducer was deposited on the bolt under these conditions. Because the bolt length is considerably greater than the thickness of the stainless-steel sheet, the ZnO deposition time on the bolt was increased to 8 h to compensate for ultrasonic attenuation over the longer propagation path. As the preload of the hydraulic bolt is primarily axial, calibration tests were performed under different axial loads at 19 °C. The longitudinal-wave velocity was calculated from the relationship between ultrasonic time-of-flight and bolt length, further demonstrating the applicability of the ZnO transducer fabricated by RF magnetron sputtering. The relationship between the applied axial load and the peak time-of-flight of the first echo is presented in Figure 10a. As the axial load increases, the ultrasonic echo TOF will be delayed. This is mainly caused by two reasons: one is that the overall length of the bolt changes under the loading condition, resulting in an increase in the ultrasonic propagation distance; the other is that according to the acoustic elasticity theory, the ultrasonic longitudinal wave is more sensitive to forces parallel to the propagation direction, so in the axial tensile stress condition, the ultrasonic propagation speed will decrease [11,31,32]. With a linear fit of the axial load and TOF, a strong correlation was shown, with an R^2 value greater than 99.99%. In the elastic loading range, the axial elongation of the bolt is proportional to the applied load according to Hooke's law, and the ultrasonic propagation distance therefore increases linearly with load. To verify the accuracy of this ultrasonic method for axial stress of the bolt, the absolute and relative error values of the bolt under different loads were calculated. The results are shown in Figure 10b. The results indicate that in the lower load range, the relative error and absolute error are relatively high, which may be due to the reduced control accuracy of the universal testing machine under low load conditions. The absolute load error remains within the ±3 kN range. With the increase in load, the relative error is always lower than 1% of the applied load. The average error for the entire load range of the bolt is controlled within 1%. The obtained linearity and measurement accuracy are comparable to those reported for previously developed ZnO-based ultrasonic bolt sensors, which have demonstrated the feasibility of determining bolt preload from ultrasonic time-of-flight under laboratory conditions. However, most previous studies focused on transducer fabrication and short-term load calibration. In the present work, the optimized sensor achieved $R^2 > 99.99\%$ and an average measurement error below 1%, and was further evaluated through approximately 200 days of field monitoring at a hydropower station. Therefore, the present study extends ZnO thin-film ultrasonic bolt sensing from laboratory verification to long-term in-service monitoring.

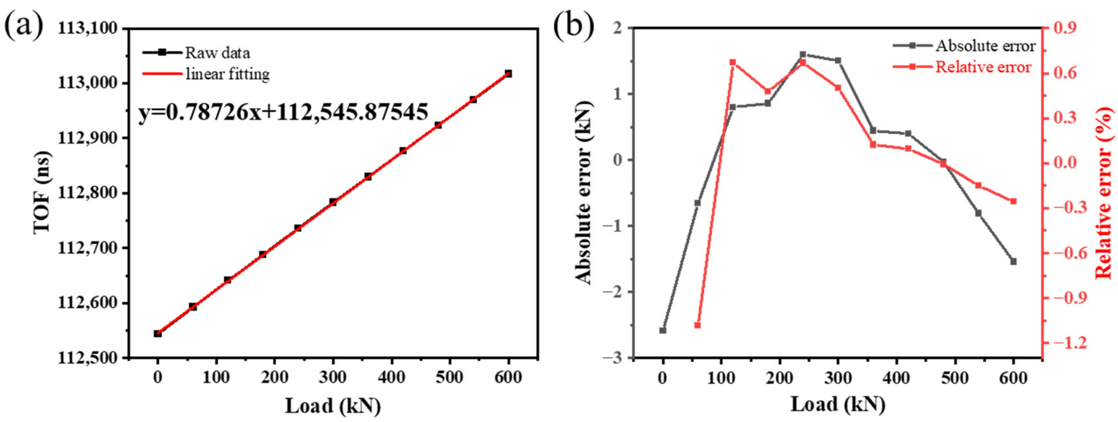

Figure 10. ZnO thin film transducers deposited on bolts. (**a**) Relationship between loads and TOF at 19 °C; (**b**) relative error and absolute error of load.

Figure 11 shows the preload variation of four randomly selected bolts and the corresponding temperature variation during field application after ZnO thin-film sensors were fabricated on the bolt surfaces at a hydropower station. Prior to monitoring, temperature calibration was performed on the bolts, and the influence of temperature on the acoustic time-of-flight was corrected during preload estimation. Therefore, the force variation shown in the Figure 11 mainly reflects the actual mechanical response of the bolted joint system under in-service conditions. As the field temperature decreased from approximately 26 °C to 12 °C, the preload variations of the bolts generally increased, with a maximum increment of about 40 kN. When the temperature subsequently increased to approximately 20 °C, the preload variation decreased significantly, indicating a negative correlation between bolt preload and temperature. This phenomenon can be attributed to the difference in thermal expansion properties between the bolt and the flange materials. The flange was made of Q235-B steel, with a linear thermal expansion coefficient of 8×10^{-6} °C^{-1}, whereas the bolt was made of 35 CrMo steel, with a linear thermal expansion coefficient of 12.5×10^{-6} °C^{-1}. During cooling, the free thermal contraction of the bolt was greater than that of the flange. Under the constraint of the joint stiffness, this thermal deformation mismatch generated an additional axial tensile force, thereby increasing the bolt preload. Conversely, as the temperature increased, the thermal deformation mismatch decreased, resulting in a reduction in preload. Compared with the specified preload of 600 kN, the observed preload variation accounted for approximately 6.7%, indicating that field temperature variation can induce non-negligible preload fluctuations. Although the four bolts exhibited certain differences in variation amplitude, their overall trends were consistent, and no abnormal sudden change or continuous preload loss was observed during the monitoring period, suggesting that the bolted connection remained stable. Compared with the conventional torque method, the proposed method can more directly characterize the axial force variation of bolts during service, and the temperature correction improves the reliability of preload estimation, demonstrating favorable measurement accuracy in field applications.

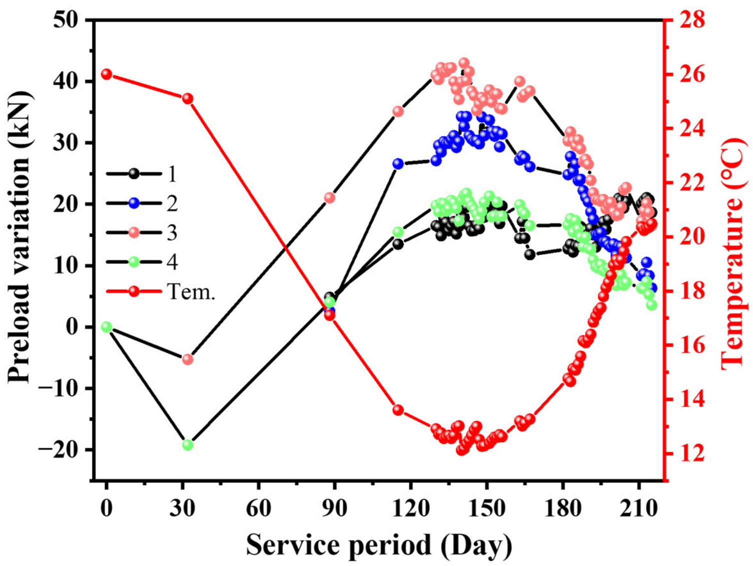

Figure 11. Variations in preload and temperature of randomly selected bolts under field service conditions.

4. Conclusions

In this study, ZnO thin-film ultrasonic transducers were prepared by reactive radio-frequency magnetron sputtering and applied to the preload measurement and field monitoring of hydropower bolts. The deposition parameters were found to play a decisive role in regulating the microstructure, crystal orientation, piezoelectric response, and ultrasonic performance of the ZnO films. With increasing deposition pressure, the growth behavior of the film gradually changed, and the ZnO film deposited at 2.0 Pa exhibited strong c-axis preferred orientation, dense columnar growth, and improved crystallization quality, which were beneficial for the excitation of longitudinal ultrasonic waves. Under this optimized pressure, further adjustment of the Ar/O_2 ratio showed that increasing the Ar partial pressure enhanced the ultrasonic signal amplitude and piezoelectric response. At an Ar/O_2 ratio of 3:1, the film showed the strongest c-axis orientation, the highest ultrasonic response, and stable high-frequency longitudinal wave excitation with a center frequency higher than 50 MHz.

The optimized ZnO thin-film transducer was directly deposited on the bolt surface to verify its preload detection capability. Based on the acoustoelastic effect, the ultrasonic time-of-flight showed a highly linear relationship with the applied axial load, with an R^2 value greater than 99.99%. Within the preload range, the average measurement error was less than 1%, indicating that the deposited ZnO thin-film transducer possessed good stability and high measurement accuracy for bolt axial force detection. Field application results further confirmed the practical feasibility of the proposed method. During in-service monitoring at a hydropower station, the preload variations of randomly selected bolts showed a clear negative correlation with temperature, which was mainly attributed to the thermal expansion mismatch between the 35CrMo bolts and Q235-B flanges. The maximum preload variation was approximately 40 kN, corresponding to about 6.7% of the specified preload of 600 kN. Although the monitored bolts exhibited certain differences in variation amplitude, their overall trends were consistent, and no abnormal sudden change or continuous preload loss was observed during the monitoring period, indicating that the bolted connection remained stable.

Overall, the proposed ZnO thin-film ultrasonic transducer can directly characterize the actual axial force state of bolts during service and effectively capture preload fluctuations caused by environmental temperature changes. Compared with conventional torque-based methods, this method avoids indirect preload estimation based on friction-dependent torque and improves the reliability of preload evaluation through ultrasonic time-of-flight measurement and temperature correction. Therefore, it provides a practical and accurate technical solution for long-term online monitoring and safety assessment of hydropower turbine bolts.

Author Contributions: Conceptualization, A.X.; Methodology, W.L. and A.X.; Software, X.J. and A.X.; Validation, W.L.; Formal analysis, X.J. and Y.J.; Resources, W.L.; Data curation, A.X.; Writing—original draft, X.J. and Y.J.; Writing—review & editing, Y.J. and J.Z.; Supervision, J.Z.; Project administration, J.Z.; Funding acquisition, W.L. and J.Z. All authors have read and agreed to the published version of the manuscript.

Funding: This work was supported by the fund project of State Grid Hunan Electric Power Company Limited Research Institute (5216A525000X).

Data Availability Statement: Data are contained within this article.

Conflicts of Interest: Authors Xuechao Jing, Wenbo Li and Ameng Xie were employed by State Grid Hunan Electric Power Company Limited Research Institute. The remaining authors declare that the research was conducted in the absence of any commercial or financial relationships that could be construed as a potential conflict of interest.

References

1. Jia, H.; Wang, D.; Xu, X.; Yu, X. Research on Some Key Problems Related to Integrated Energy Systems. *Autom. Electr. Power Syst.* **2015**, *39*, 198–207.
2. Li, H.; Liu, D.; Yao, D. Analysis and reflection on the development of power system towards the goal of carbon emission peak and carbon neutrality. *Proc. CSEE* **2021**, *41*, 6245–6259.

3. Ma, Z.Y.; Chen, H.Y.; Zhang, H.Z. 60188 The coupled dynamic analysis of hydroelectric unit and powerhouse considering the bolt connection characteristics. In *IOP Conference Series: Earth and Environmental Science*; IOP Publishing: Bristol, UK, 2021; Volume 774, p. 012039.
4. Xu, Y.; Jiang, Y.; Tan, K.; Yang, W.; Lv, J.; Deng, D.; Zheng, D.; Li, C.; Zhang, J.; Yang, B. Preparation of ZnO Ultrasonic Transducer by Radio-Frequency Sputtering and Its Application in Bolt Preload Detection. *Coatings* **2024**, *14*, 718.
5. Zhang, Y.; Jiang, Y.; Ma, C.; Zhang, J.; Yang, B. Preparation of ZnO piezoelectric thin-film material for ultrasonic transducers applied in bolt stress measurement. *Coatings* **2023**, *13*, 1538. [CrossRef]
6. Yadavar, N.S.M.; Masoud, G. A Review Paper on Looseness Detection Methods in Bolted Structures. *Lat. Am. J. Solids Struct.* **2017**, *14*, 2153–2176. [CrossRef]
7. Chen, P.; He, X.; Song, W. Parameter Recognition of Mode-Converted Wave in Single-Source Ultrasound Using Gabor Transform for Bolt Axial Stress Evaluation. *J. Sens.* **2020**, *2020*, 8883845. [CrossRef]
8. Wang, Z.; Liu, M.; Zhou, Z.; Qu, Y.; Wei, Q.; Hong, L.; Yang, F. An FBG based smart clamp for the detection of incipient clamp looseness in industrial piping system. *Measurement* **2019**, *140*, 416–426. [CrossRef]
9. Liu, Y.; Liu, E.; Chen, Y.; Wang, X.; Sun, C.; Tan, J. Measurement of fastening force using dry-coupled ultrasonic waves. *Ultrasonics* **2020**, *108*, 106178. [CrossRef]
10. Pan, Q.; Pan, R.; Chang, M.; Xu, X. A shape factor based ultrasonic measurement method for determination of bolt preload. *NDT E Int.* **2020**, *111*, 102210. [CrossRef]
11. Huang, J.; Liu, J.; Gong, H.; Deng, X.J.M.S.; Processing, S. A comprehensive review of loosening detection methods for threaded fasteners. *Mech. Syst. Signal Process.* **2022**, *168*, 108652. [CrossRef]
12. Zeng, X.; Zhang, X.; Pelenovich, V.; Neena, D.; Xu, C.; Liu, Y.; Jiang, Y.; Zeng, L.; Pogrebnjak, A.; Vildanov, R.J.C.I. High-temperature thin film lithium niobium oxide transducers for bolts. *Ceram. Int.* **2023**, *49*, 7710–7716. [CrossRef]
13. Jiang, Y.; Li, J.; Jiao, G.; Li, W.; Liu, Y.; Wang, C.; Xia, B.; Wan, B.; Zhang, J.; Pelenovich, V.; et al. ZnO piezoelectric coatings used for the ultrasonic excitation of longitudinal-transverse waves and their application for smart bolts. *J. Vac. Sci. Technol. B* **2022**, *40*, 043002. [CrossRef]
14. Xu, T.; Wu, G.; Zhang, G.; Hao, Y. The compatibility of ZnO piezoelectric film with micromachining process. *Sens. Actuators A Phys.* **2003**, *104*, 61–67. [CrossRef]
15. Dahmani, H.; Zaaroura, I.; Salhab, A.; Campistron, P.; Carlier, J.; Toubal, M.; Harmand, S.; Thomy, V.; Neyens, M.; Nongaillard, B. Fabrication and optimization of high frequency ZnO transducers for both longitudinal and shear emission: Application of viscosity measurement using ultrasound. *Adv. Sci. Technol. Eng. Syst. J.* **2020**, *5*, 1428–1435. [CrossRef]
16. Mitrushchenkov, A.; Linguerri, R.; Chambaud, G. Piezoelectric properties of AlN, ZnO, and $Hg_xZn_{1-x}O$ nanowires by first-principles calculations. *J. Phys. Chem. C* **2009**, *113*, 6883–6886. [CrossRef]
17. Al-Khawaja, S.; Abdallah, B.; Abou Shaker, S.; Kakhia, M. Thickness effect on stress, structural, electrical and sensing properties of (0 0 2) preferentially oriented undoped ZnO thin films. *Compos. Interfaces* **2015**, *22*, 221–231. [CrossRef]
18. Luo, J.; Quan, A.; Fu, C.; Li, H. Shear-horizontal surface acoustic wave characteristics of a (110) $ZnO/SiO_2/Si$ multilayer structure. *J. Alloys Compd.* **2017**, *693*, 558–564. [CrossRef]
19. Kumar, R.; Kumar, G.; Al-Dossary, O.; Umar, A. ZnO nanostructured thin films: Depositions, properties and applications—A review. *Mater. Express* **2015**, *5*, 3–23. [CrossRef]
20. Bussell, B.C.; Gibson, P.N.; Lawton, J.; Couture, P.; Sharpe, M.; England, J.; Hinder, S.; Stolojan, V.; Thornley, S.; Baker, M. The effect of RF plasma power on remote plasma sputtered AZO thin films. *Surf. Coat. Technol.* **2022**, *442*, 128402. [CrossRef]
21. Lu, J.; Ye, Z.; Huang, J.; Wang, L.; Zhao, B. Synthesis and properties of ZnO films with (1 0 0) orientation by SS-CVD. *Appl. Surf. Sci.* **2003**, *207*, 295–299. [CrossRef]
22. Lee, J.H.; Song, J.T. Dependence of the electrical and optical properties on the bias voltage for ZnO:Al films deposited by r.f. magnetron sputtering. *Thin Solid Films* **2008**, *516*, 1377–1381. [CrossRef]
23. Greene, J. Thin film nucleation, growth, and microstructural evolution: An atomic scale view. In *Handbook of Deposition Technologies for Films and Coatings*; Elsevier: Amsterdam, The Netherlands, 2010; pp. 554–620.
24. Wu, S.; Lin, Z.-X.; Lee, M.-S.; Ro, R. Bulk acoustic wave analysis of crystalline plane oriented ZnO films. *J. Appl. Phys.* **2007**, *102*, 084908. [CrossRef]
25. Tao, Y.; Ma, S.; Chen, H.; Meng, J.; Hou, L.; Jia, Y.; Shang, X. Effect of the oxygen partial pressure on the microstructure and optical properties of ZnO: Cu films. *Vacuum* **2011**, *85*, 744–748. [CrossRef]
26. Song, D.; Aberle, A.G.; Xia, J. Optimisation of ZnO: Al films by change of sputter gas pressure for solar cell application. *Appl. Surf. Sci.* **2002**, *195*, 291–296. [CrossRef]
27. Ali, Z.; Afzal, N.; Rafique, M. Effect of Ar: O_2 ratio on reactively magnetron sputtered ZnO film's properties. *Mater. Res. Express* **2019**, *6*, 116419. [CrossRef]
28. Kim, S.S.; Lee, B.-T. Effects of oxygen pressure on the growth of pulsed laser deposited ZnO films on Si (0 0 1). *Thin Solid Film.* **2004**, *446*, 307–312. [CrossRef]

29. Ali, W.R.; Prasad, M. Piezoelectric MEMS based acoustic sensors: A review. *Sens. Actuators A Phys.* **2020**, *301*, 111756. [CrossRef]
30. Wall, J.M.; Yan, F. Sputtering process of $Sc_xAl_{1-x}N$ thin films for ferroelectric applications. *Coatings* **2022**, *13*, 54. [CrossRef]
31. Zhao, X.X.; Li, Y.M.; Liu, X.G.; Yao, K. Ultrasonic measurement on axial force of high-strength bolt in service. *J. Low Freq. Noise Vib. Act. Control* **2020**, *39*, 596–603.
32. Liu, W.; Shan, L.; Lin, Z.; Wan, B.; Yang, B.; Zeng, X.; Yang, B.; Pelenovich, V. Dual-Wave ZnO Film Ultrasonic Transducers for Temperature and Stress Measurements. *Sensors* **2024**, *24*, 5691. [CrossRef] [PubMed]